
Label Embedding by Johnson-Lindenstrauss Matrices

Jianxin Zhang and Clayton Scott
Electrical Engineering and Computer Science
University of Michigan
Ann Arbor, MI 48109
{jianxinz, clayscot}@umich.edu

Abstract

We present a simple and scalable framework for extreme multiclass classification based on Johnson-Lindenstrauss matrices (JLMs). Using the columns of a JLM to embed the labels, a C -class classification problem is transformed into a regression problem with $\mathcal{O}(\log C)$ output dimension. We derive an excess risk bound, revealing a tradeoff between computational efficiency and prediction accuracy, and further show that under the Massart noise condition, the penalty for dimension reduction vanishes. Our approach is easily parallelizable, and experimental results demonstrate its effectiveness and scalability in large-scale applications.

1 Introduction

Extreme classification refers to multiclass and multilabel classification problems involving thousands of classes or more, and has emerged as an essential research area in machine learning. This is due to an increasing number of real-world applications involving massive numbers of classes, such as image recognition (Zhou et al., 2014), natural language processing (Le and Mikolov, 2014; Jernite et al., 2017), and recommendation systems (Bhatia et al., 2015; Chang et al., 2019). Traditional classification methods often struggle to scale effectively in these scenarios due to the high computational cost and memory requirements associated with handling large label spaces. Consequently, there is a growing need for efficient and scalable algorithms that can tackle extreme classification problems without compromising on performance (Prabhu and Varma, 2014; Prabhu et al., 2018; Deng et al., 2018).

In this paper, we introduce a simple and scalable framework for extreme multiclass classification using Johnson-Lindenstrauss random matrices. Our approach transforms the original C -class classification problem into a regression problem with $\mathcal{O}(\log C)$ output dimension, substantially reducing computational complexity while preserving classification performance. The cornerstone of our framework is the use of the columns of a Johnson-Lindenstrauss random matrix as class-representative embedding vectors. Learning simply involves fitting a regression model to predict the embedded label of an instance, and our framework is thus compatible with any multi-output regression model, such as linear models, random forests, and neural networks. Given a test instance, the predicted label is the label of the nearest embedding vector to the output of the fitted regression model.

A key contribution of this work is the derivation of an excess risk bound, offering theoretical guarantees for the performance of the proposed method. The bound reveals a tradeoff between computational efficiency and classification accuracy, wherein a logarithmic reduction in the output space dimension incurs only a small penalty in prediction accuracy. Furthermore, under the multiclass noise condition of Massart and Nédélec (2006), the penalty for dimension reduction vanishes. In addition to these performance guarantees, our approach is easily parallelizable, making it an attractive solution for large-scale applications that demand efficient processing. We validate the effectiveness and scalability of our proposed method through a series of experiments on various real-world datasets, demonstrating its potential to address the challenges posed by extreme multiclass classification tasks.

The remainder of this paper is organized as follows: Section 2 introduces related work on extreme multiclass classification. Section 3 reviews Johnson-Lindenstrauss matrices. Section 4 presents our proposed framework in detail along with the excess risk bound. Section 5 presents experimental results and evaluations. Finally, Section 6 concludes the paper and outlines future research directions.

2 Related Work

Existing methods for extreme multiclass classification can be grouped into four main categories: Label Hierarchy, Label Embedding, One-vs-all methods, and other methods.

Label Hierarchy. Numerous methods such as Parabel (Prabhu et al., 2018), Bonsai (Khandagale et al., 2020), AttentionXML (You et al., 2019), lightXML (Jiang et al., 2021), XR-Transformer (Zhang et al., 2021), X-Transformer (Wei et al., 2019), XR-Linear (Yu et al., 2022), and ELIAS (Gupta et al., 2022) partition the label spaces into clusters. This is typically achieved by performing k -means clustering on the feature space. The training process involves training a cluster-level model to assign a cluster to a feature vector, followed by training a label-level model to assign labels within the cluster. As each cluster contains a relatively small number of labels, the training cost is effectively reduced. Notably, Parabel (Prabhu et al., 2018) represents labels using binary trees where each node represents a label cluster, and its children represent exclusive subsets of their parent. ELIAS (Gupta et al., 2022) allows label clusters to overlap and updates label-cluster assignments during training. However, a potential drawback of such methods that construct a label hierarchy is the often noticeable absence of robust theoretical support.

Label Embedding. A natural approach involves representing each label as a vector in a low-dimensional space. LEML (Yu et al., 2014) leverages a low-rank assumption on linear models and effectively constrains the output space of models to a low-dimensional space. SLICE (Jain et al., 2019) is designed to train on low-dimensional dense features, with each label represented by the mean of all feature vectors associated with that label. SLEEC (Bhatia et al., 2015) proposes a local embedding framework that preserves the distance between label vectors. Guo et al. (2019) point out that low-dimensional embedding-based models could suffer from significant overfitting. Their theoretical insights inspire a novel regularization technique to alleviate overfitting in embedding-based models. WLSTS (Evron et al., 2018) proposes an extreme multiclass classification framework based on *error correcting output coding*, which embeds labels with codes induced by graphs. Hsu et al. (2009) use column vectors from a matrix with the *restricted isometry property* (RIP), which is satisfied by all Johnson Lindenstrauss matrices, to represent labels. Their analysis is primarily tailored to multilabel classification and rooted in a compressed sensing framework. They deduce bounds for the conditional ℓ_2 -error, which measures the 2-norm difference between the prediction and the label vector — a metric that is not a standard measure of classification error. In contrast, our work analyzes the standard classification error. Embedding-based methods generally underperform compared to state-of-the-art approaches in empirical evaluations.

One-vs-all methods. One-vs-all (OVA) algorithms address extreme classification problems with C labels by modeling them as C independent binary classification problems. For each label, a classifier is trained to predict its presence. DiSMEC (Babbar and Schölkopf, 2017) introduces a large-scale distributed framework to train linear OVA models, albeit at an expensive computational cost. ProXML (Babbar and Schölkopf, 2019) formulates the extreme classification problem as robust learning with adversarial perturbations to mitigate the impact of data scarcity. PD-Sparse (Yen et al., 2016) assumes both feature vectors and label vectors are sparse and designs an optimization algorithm to fully exploit the sparsity. PPD-Sparse (Yen et al., 2017) proposes a parallelized version of PD-Sparse.

Other methods. Beyond the above categories, DeepXML (Dahiya et al., 2021) proposes a framework based on a negative sampling procedure that shortlists $O(\log C)$ relevant labels during training and prediction, where C is the total number of labels. VM (Choromanska and Langford, 2015) constructs trees with $\mathcal{O}(\log C)$ depth that have leaves with low label entropy. Based on the standard random forest training algorithm, FastXML (Prabhu and Varma, 2014) proposes to directly optimize the Discounted Cumulative Gain to reduce the training cost. AnnexML (Tagami, 2017) constructs k -nearest neighbor graph of the label vectors and attempts to reproduce the graph structure in a lower-dimension feature space.

We now mention theoretical contributions that are most related to our own. The seminal work of Allwein et al. (2001) generalizes the *error correcting output codes* (ECOC) framework for multiclass

classification, transforming the problem into multiple binary classification tasks. The authors establish a bound on the empirical multiclass loss based on the empirical loss of the individual binary learners and present a generalization error analysis when AdaBoost is employed as the binary learner. Drawing inspiration from the error bound proposed by Allwein et al. (2001), Evron et al. (2018) applies the ECOC principle to extreme multiclass classification. In their approach, labels are embedded with codes that are generated by graphs. In a different perspective, Ramaswamy et al. (2018) put forth a novel surrogate loss function for multiclass classification with an abstain option. This abstain option enables the classifier to opt-out from making predictions at a certain cost. Remarkably, their proposed methods not only demonstrate consistency but also effectively reduce the multiclass problems to $\lceil \log C \rceil$ binary classification problems through encoding the classes with their binary representations. Our research can be interpreted as a continuous refinement of the concept of reducing multiclass problems to binary problems. We transform multiclass problems into regression problems on a $\mathcal{O}(\log C)$ space. Crucially, our excess risk analysis unveils the intricate balance between statistical and computational efficiency.

3 Johnson-Lindenstrauss Matrices

We first review the definition of a Johnson-Lindenstrauss matrix.

Definition 1. Let $C, n \in \mathbb{N}$. We define the set of $C \times n$ Johnson-Lindenstrauss matrices with parameters ϵ, δ, m , denoted by $\text{JLM}(\epsilon, \delta, m)$, to be the set of $C \times n$ random matrices such $G \in \text{JLM}(\epsilon, \delta, m)$ if and only if, with probability at least $1 - \delta$, $\forall m$ -element subsets $V \subset \mathbb{R}^n, \forall v, v' \in V$, $|\langle Gv, Gv' \rangle - \langle v, v' \rangle| \leq \epsilon \|v\| \|v'\|$.

Johnson-Lindenstrauss matrices have approximately orthonormal columns, meaning each column has approximately unit norm and every two distinct columns have inner-product close to 0. In the standard approach to multiclass classification, labels can be viewed as embedded by the standard basis. Our framework, instead, embeds labels by the approximately orthonormal columns of a Johnson-Lindenstrauss matrix, where the embedding dimension is n . Popular choices of Johnson-Lindenstrauss matrices include:

- Gaussian matrix: entries are sampled *i.i.d.* from a Gaussian distribution with 0 mean and $\frac{1}{n}$ variance.
- Rademacher matrix: entries are sampled *i.i.d.* from a uniform distribution on $\left\{ \frac{1}{\sqrt{n}}, -\frac{1}{\sqrt{n}} \right\}$.

The above examples are Johnson-Lindenstrauss matrices with shape $C \times n$ and parameters ϵ, δ, m if $n \geq \frac{c_0}{\epsilon^2} \log \frac{m}{\delta}$ for some constant c_0 (Johnson and Lindenstrauss, 1984).

In our embedding framework, the Johnson-Lindenstrauss matrix has dimensions $C \times n$, where C is the total number of classes and n is the embedding dimension chosen by the user. The matrix is designed to embed a C -element set of vectors in \mathbb{R}^C , in particular the standard basis, which makes $m = C$, allowing for a reduction of the output dimension to $\mathcal{O}(\log C)$.

4 Label Embedding by Johnson-Lindenstrauss Matrices

We first introduce the notations in Section 4.1. Then, we present our algorithm in Section 4.2. The excess risk bound and its interpretation are presented in Section 4.3.

4.1 Preliminaries

Let \mathcal{X} denote the feature space and $\mathcal{Y} = \{1, \dots, C\}$ denote the label space where $C \in \mathbb{N}$. Let (X, Y) be random variables in $\mathcal{X} \times \mathcal{Y}$, and let P be the probability measure that governs (X, Y) . We use $P_{\mathcal{X}}$ to denote the marginal distribution of P on \mathcal{X} . Now, consider a $C \times n$ matrix $G \in \text{JLM}(\epsilon, \delta, C)$. The columns of G are denoted by g_1, g_2, \dots, g_C , and the column g_i is used to embed the i -th label. With this setup, our goal is to transform the original C -class classification problem into a regression problem with $\mathcal{O}(\log C)$ outputs. For this, let $\mathcal{F} = \{\text{all measurable } f : \mathcal{X} \rightarrow \mathbb{R}^n\}$ and let $\eta(x) = (\eta_1(x), \dots, \eta_C(x))$, where $\eta_i(x) = P_{Y|X=x}(i)$. This flexible regression model setup enables our framework to be compatible with any model class. Let $\beta(p) : \mathbb{R}^n \rightarrow \mathcal{Y}, \beta(p) =$

Algorithm 1 Label Embedding for Extreme Multiclass Classification

- 1: **Input:** a model class $\mathcal{F}_0 \in \mathcal{F}$, the dataset $\mathcal{D} = \{(x_i, y_i)\}_{i=1}^N$, and embedding dimension n .
 - 2: Sample a $C \times n$ Johnson-Lindenstrauss matrix with columns g_1, g_2, \dots, g_C .
 - 3: Form the new regression dataset $\mathcal{D}_r = \{(x_i, g_{y_i})\}_{i=1}^N$.
 - 4: Train a regression model f on \mathcal{D}_r with mean square error ℓ .
 - 5: **Return:** $\beta \circ f$.
-

$\min\{\arg \min_{i \in \mathcal{Y}} \|p - g_i\|_2\}$ be the decoding function, which maps a vector in the embedding space back to its corresponding label, where p is the output of a model. The corresponding label is determined by identifying the nearest embedding vector to p . In the rare case where multiple nearest neighbors exist for p , we resolve this ambiguity by considering the lexicographical order of the labels that they represent. In such cases, the function β returns the smallest label from the set of labels corresponding to the nearest embedding vectors.

Define the 0-1 loss $L_{01} : \mathcal{Y} \times \mathcal{Y} \rightarrow \mathbb{R}$ to be $L_{01}(\hat{y}, y) = \begin{cases} 1, & \text{if } y \neq \hat{y} \\ 0, & \text{o.w.} \end{cases}$. The standard objective

for classification is to solve $\min_{h \in \mathcal{H}} \mathbb{E}[L_{01}(h(X), Y)]$, where $\mathcal{H} = \{\text{measurable } h : \mathcal{X} \rightarrow \mathcal{Y}\}$ is the set of all measurable functions \mathcal{X} to \mathcal{Y} . We now claim that $\beta \circ \mathcal{F}$ reparameterizes \mathcal{H} , which stems from the following facts: (i) for any given $f \in \mathcal{F}$, the function $\beta \circ f$ is also measurable, (ii) for all $h \in \mathcal{H}$, the function $f(x) = g_{h(x)}$ ensures that $\beta \circ f = h$, and (iii) such f are measurable because \forall measurable sets \mathcal{S} , $f^{-1}(\mathcal{S}) = \bigcup_{i: g_i \in \mathcal{S}} h^{-1}(i)$. Thus, the problem $\min_{f \in \mathcal{F}} \mathbb{E}_P[L_{01}(\beta(f(X)), Y)]$ is equivalent to the standard classification objective. To simplify notation, we introduce the loss function $L : \mathbb{R}^n \times \mathcal{Y}$, such that $L(p, y) = L_{01}(\beta(p), y)$. As a result, our learning objective can be equivalently written as $\min_{f \in \mathcal{F}} \mathbb{E}_P[L(f(X), Y)]$.

Given the impracticality of directly minimizing the 0-1 loss, we consider instead the surrogate loss function $\ell : \mathbb{R}^n \times \mathcal{Y} \rightarrow \mathbb{R}$, defined as $\ell(p, y) = \frac{1}{2} \|p - g_y\|_2^2$, and aim to optimize $\mathbb{E}_P[\ell(f(X), g_Y)]$ over a specific model class $\mathcal{F}_0 \subset \mathcal{F}$ through empirical risk minimization. Following the introduction of our learning algorithm, we will present an analysis of excess risk for L , in terms of the excess risk associated with the surrogate loss function ℓ .

4.2 Algorithm

Let the training dataset $\{(x_i, y_i)\}_{i=1}^N$ be *i.i.d.* realizations of (X, Y) . To train a model that maps a feature vector to a vector in the embedding space, we first sample a $C \times n$ Johnson-Lindenstrauss matrix $G = [g_1, g_2, \dots, g_C]$. We then replace each label y_i with its embedding vector g_{y_i} to form the regression dataset $\{(x_i, g_{y_i})\}_{i=1}^N$. Next, we train a regression model f on this regression dataset. Given a new data point x , to assign a label we search for the nearest embedding vector g_y of $f(x)$ and annotate x with the label y . The full algorithm is presented in Algorithm 1. It is crucial to emphasize that the regression step in Algorithm 1 is a regression problem with a response in \mathbb{R}^n . This enables a novel parallel training scheme that distributes the response variables across a maximum of n machines without any need of inter-machine communication. Each machine is tasked with solving one or a small number of real-valued regression problems. We employ this parallel training scheme in the elastic net implementation of our framework in the experiments.

4.3 Excess Risk Bound

We present the excess risk bound and examine the trade-off between the reduction in dimensionality and the potential penalty in accuracy. Before delving into the excess risk analysis, we first introduce the concepts of *risk* and *Bayes risk*.

Definition 2. Let $\mathcal{L} : \mathbb{R}^n \times \mathcal{Y} \rightarrow \mathbb{R}$. Define the \mathcal{L} -risk of f with distribution P to be

$$\mathcal{R}_{\mathcal{L}, P} : \mathcal{F} \rightarrow \mathbb{R}, \quad \mathcal{R}_{\mathcal{L}, P}(f) := \mathbb{E}_P[\mathcal{L}(f(X), Y)]$$

and the \mathcal{L} -Bayes risk to be

$$\mathcal{R}_{\mathcal{L}, P}^* := \inf_{f \in \mathcal{F}} \mathcal{R}_{\mathcal{L}, P}(f).$$

We define $d(x) = \max_i \eta_i(x) - \max_{i \notin \arg \max_j \eta_j(x)} \eta_i(x)$. $d(x)$ is a ‘‘noise’’ measure at a point x and we discuss it after Theorem 3. The bound is as follows:

Theorem 3. *Let $\delta, \epsilon \in (0, 1)$. If $G \in JLM(\frac{\epsilon}{4}, \delta, C)$, then with probability at least $1 - \delta$,*

$$\mathcal{R}_{L,P}(f) - \mathcal{R}_{L,P}^* \leq \inf_{r > \epsilon} \left\{ \epsilon P_{\mathcal{X}}(d(X) < r) \right. \quad (1)$$

$$\left. + \sqrt{(8\epsilon + 16)P_{\mathcal{X}}(d(X) < r) \left(\mathcal{R}_{\ell,P}(f) - \mathcal{R}_{\ell,P}^* \right)} \right. \quad (2)$$

$$\left. + \frac{16 + 8\epsilon}{(r - \epsilon)^2} \left(\mathcal{R}_{\ell,P}(f) - \mathcal{R}_{\ell,P}^* \right) \right\}. \quad (3)$$

Prior to delving into the proof sketch, we first explicate the concept of *conditional risk*. The full proofs and associated lemmas are provided in the appendix. The remarks on the theorem and the quantity $d(x)$ will come after the proof sketch.

Definition 4. Let $\mathcal{L} : \mathbb{R}^n \times \mathcal{Y} \rightarrow \mathbb{R}$ be a loss function and P be a probability measure on $\mathcal{X} \times \mathcal{Y}$. For a point $x \in \mathcal{X}$, define the conditional risk at x as

$$C_{\mathcal{L},x} : \mathbb{R}^n \rightarrow \mathbb{R}, C_{\mathcal{L},x}(p) = \mathbb{E}_{y \sim P_{\mathcal{Y}|X=x}} \mathcal{L}(p, g_y),$$

and $C_{\mathcal{L},x}^* = \inf_{p \in \mathbb{R}^n} C_{\mathcal{L},x}(p)$.

The conditional risk represents the expected value of a loss given the model output p and a feature vector x . Note that $\mathcal{R}_{\mathcal{L},P}(f) = \mathbb{E}_{X \sim P_{\mathcal{X}}} C_{\mathcal{L},X}(f(X))$. For brevity, we introduce the notations $C_{1,x}(p) = C_{L,x}(p) - C_{L,x}^*$, $C_{2,x}(p) = C_{\ell,x}(p) - C_{\ell,x}^*$.

Proof outline for Theorem 3. We begin by demonstrating in Lemma 10 that there exists a unique p_x^* such that $C_{\ell,x}^* = C_{\ell,x}(p_x^*)$. Here, p_x^* represents the optimal model output at a specific point x . Utilizing the Johnson-Lindenstrauss property of the embedding matrix, we establish in Lemma 13 that:

$$\forall x \in \mathcal{X}, \forall j, k \in [C], \forall p \in \mathbb{R}^n, \frac{\eta_k(x) - \eta_j(x) - \epsilon}{2\sqrt{2} + \epsilon} > \|p_x^* - p\| \implies \|p - g_j\|_2 > \|p - g_k\|_2.$$

This implies that if a model output p is sufficiently close to p_x^* and the probability $\eta_k(x)$ for label k to occur exceeds the probability $\eta_j(x)$ for label j by a some margin, then p is closer to g_k than to g_j .

By leveraging the above property along with the convexity of $C_{2,x}$, we demonstrate in Lemma 14 that:

$$\forall x \in \mathcal{X}, \forall r > \epsilon, \forall p \in \mathbb{R}^n, C_{2,x}(p) < \frac{(r - \epsilon)^2}{16 + 8\epsilon} \implies C_{1,x}(p) < r. \quad (4)$$

This means a small $C_{2,x}(p)$ will lead to a small $C_{1,x}(p)$ up to the noise tolerance ϵ .

The final step involves expressing the excess risk as

$$\mathcal{R}_{L,P}(f) - \mathcal{R}_{L,P}^* = \int_{\mathcal{X}} C_{1,x}(f(x)) = \int_{x:d(x) < r} C_{1,x}(f(x)) + \int_{x:d(x) \geq r} C_{1,x}(f(x)).$$

By plugging (4) into the integral, the first integral leads to terms (1) and (2) and the second integral leads to term (3). \square

The excess risk $\mathcal{R}_{L,P}(f) - \mathcal{R}_{L,P}^*$ measures the gap between the L -risk of f and the Bayes risk. Our aim is to minimize $\mathcal{R}_{L,P}(f) - \mathcal{R}_{L,P}^*$ by driving the quantity $\mathcal{R}_{\ell,P}(f) - \mathcal{R}_{\ell,P}^*$ to 0 through empirical risk minimization over a sufficiently rich function space \mathcal{F}_0 . While terms (2) and (3) in Theorem 3 can be driven to 0 asymptotically through training, term (1) represents an irreducible error incurred in a ‘‘noisy’’ region of \mathcal{X} .

While $\max_i \eta_i(x)$ represents the probability of the most likely label occurring and $\max_{i \notin \arg \max_j \eta_j(x)} \eta_i(x)$ represents the probability of the second most likely label occurring, the quantity $d(x)$, which is the difference between these probabilities, can be viewed as a measure of noisiness at a point x . A large $d(x)$ implies that $\arg \max_i \eta_i(x)$ is unambiguously the correct prediction

at x . In contrast, if $d(x)$ is small, our confidence in predicting the most likely label $\arg \max_i \eta_i(x)$ is reduced, as the second most likely label has a probability of occurring that is only marginally smaller than $\max_i \eta_i(x)$. A smaller $d(x)$ highlights the increased difficulty of making accurate predictions in situations where the distinction between the most probable labels is less pronounced.

The embedding framework introduces fuzziness to the problem as a trade-off for dimensionality reduction. This fuzziness is measured by the error tolerance of the embedding matrix, ϵ . From the proof outline we can see that the model f^* minimizing the ℓ -risk $\mathcal{R}_{L,P}(f)$ may potentially make a suboptimal prediction at point x when $d(x) < \epsilon$. Conversely, when $d(x) > \epsilon$, f^* will always make the optimal prediction at point x . Given a classification problem with C classes, a larger embedding dimension n will lead to a smaller error tolerance ϵ , making $d(x) > \epsilon$ on a larger region in \mathcal{X} at the cost of increasing computational complexity. On the other hand, by choosing a smaller n , $d(x) < \epsilon$ on a larger region in \mathcal{X} , increasing the first term in Theorem 3. This interpretation highlights the delicate balance between the benefits of dimensionality reduction and the potential impact on prediction accuracy, as a function of the embedding error tolerance, ϵ , and the noisiness measure, $d(x)$.

4.4 Lossless Dimensionality Reduction

While Theorem 3 holds universally (for all distributions P), by considering a specific subset of distributions, we can derive a more conventional form of the excess risk bound. As a direct consequence of Theorem 3, under the multiclass extension of the Massart noise condition (Massart and Nédélec, 2006) which requires $d(X) > c$ with probability 1 for some c , our embedding framework achieves lossless logarithmic dimensionality reduction with respect to the 0-1 loss. This means that term 1 in Theorem 3 will be 0 under this condition. In this case, the difference $\mathcal{R}_{L,P}(f) - \mathcal{R}_{L,P}^*$ tends to 0 as the excess risk $\mathcal{R}_{\ell,P}(f) - \mathcal{R}_{\ell,P}^*$ also approaches 0. We present this result more formally with the following definition and corollary.

Definition 5 (Multiclass Massart Noise Condition). The distribution P on $\mathcal{X} \times \mathcal{Y}$ is said to satisfy the Multiclass Massart Noise Condition if and only if $\exists c > 0$ such that $P_{\mathcal{X}}(d(X) > c) = 1$.

Corollary 6. Assume P satisfies the Multiclass Massart Noise Condition. Let $\delta \in (0, 1)$ and $\epsilon \in (0, \text{ess inf } d)$. If $G \in \text{JLM}(\frac{\epsilon}{4}, \delta, C)$, then with probability at least $1 - \delta$,

$$\mathcal{R}_{L,P}(f) - \mathcal{R}_{L,P}^* \leq \frac{16 + 8\epsilon}{(\text{ess inf } d - \epsilon)^2} (\mathcal{R}_{\ell,P}(f) - \mathcal{R}_{\ell,P}^*)$$

where $\text{ess inf } d$ is the essential infimum of d , i.e. $\text{ess inf } d = \sup\{a \in \mathbb{R} : P_{\mathcal{X}}(d(X) < a) = 0\}$.

5 Experiments

¹ In this section, we present an experimental evaluation of our proposed embedding framework, which we call JOLLE (JOHnson-Lindenstrauss Label Embedding), on extreme multiclass classification problems. We have aimed to develop a general framework for extreme multiclass classification that is not specifically tailored to language datasets. Although methods like AttentionXML (You et al., 2019), lightXML (Jiang et al., 2021), XR-Transformer (Zhang et al., 2021), X-Transformer (Wei et al., 2019), and ELIAS (Gupta et al., 2022) have been designed for language datasets and leverage language models like BERT, our primary focus lies beyond achieving the highest performance on such datasets. Instead, we compare our method with more general approaches, including Parabel (Prabhu et al., 2018), PD-Sparse (Yen et al., 2016), PPD-Sparse (Yen et al., 2017), WLSTS (Evron et al., 2018), and AnnexML (Tagami, 2017), which are applicable across a broader range of multiclass extreme classification problems. We examine the performance of our method on three bag-of-words datasets: LSHTC1, Dmoz, and ODP. Notably, we abstain from integrating a language model into our framework due to the unavailability of raw text in these datasets, which prevents us from training a regression model on the dense feature representations extracted by language models. By evaluating our method against these general methods, we aim to demonstrate its versatility and effectiveness in various contexts.

¹Code is available at <https://github.com/Z-Jianxin/JOLLE>

5.1 Experiment Setup

We adapt our method to three widely used base models: elastic net, random forest, and fully-connected neural networks. It is important to note that elastic net is a linear method incorporating both ℓ_1 and ℓ_2 penalties. This choice of penalty is inspired by Yen et al. (2016). Elastic net and random forest are implemented in C++, both with single-node and multiprocess variants. Neural networks are implemented using Pytorch, with a 2-layer fully-connected neural network used for the LSHTC1 and DMOZ datasets and a 4-layer fully-connected neural network for the ODP dataset. We tune the hyperparameters for all models on a held-out dataset. we employ the Rademacher matrix as our embedding matrix, which has demonstrated superior empirical performance in our tests. For the competing methods, we use the hyperparameters as suggested in their respective papers or accompanying code. We conduct experiments on three large-scale datasets, DMOZ, LSHTC1, and ODP, which are extensively used for benchmarking extreme classification algorithms. The details of these datasets are provided in Table 1, with DMOZ and LSHTC1 available from Yen et al. (2016), and ODP from Medini et al. (2019).

Dataset	N_{train}	N_{test}	D	C
LSHTC1	83805	5000	328282	12046
Dmoz	335068	38340	561127	11879
ODP	975936	493014	493014	103361

Table 1: Summary of the datasets used in the experiments. Here, N_{train} is the number of training data points, N_{test} the number of test data points, D the number of features, and C the number of classes.

We compare our method against the following state-of-the-art methods:

- PD-Sparse (Yen et al., 2016): an efficient solver designed to exploit the sparsity in extreme classification.
- PPD-Sparse Yen et al. (2017): a multi-process extension of PD-Sparse (Yen et al., 2016).
- Parabel (Prabhu et al., 2018): a tree-based method which builds a label-hierarchy.
- WLSTS (Evron et al., 2018): a method based on *error correcting output coding* which embeds labels by codes induced by graphs.
- AnnexML (Tagami, 2017): a method which constructs a k -nearest neighbor graph of the label vectors and attempts to reproduce the graph structure from a lower-dimension feature space.
- Standard multilayer perceptron classifier with cross-entropy loss.
- Standard multilayer perceptron classifier with squared error loss.

All neural network training is carried out on a single NVIDIA A40 GPU with 48GB of memory, whereas all other methods are executed on Intel Xeon Gold 6154 processors, equipped with 36 cores and 180GB of memory. Our distributed approach and the PPD-Sparse method — also implemented in a distributed fashion — are trained across 10 CPU nodes, harnessing 360 cores and 1.8TB of memory in total. For our CPU-based methods, we consistently set the embedding dimension to $n = 360$. In our distributed implementation, each node independently solves a subset of elastic nets with real-value output, effectively spreading out the computation. Similarly, the random forest model is distributed by assigning each core to compute a subset of trees. For deep neural networks, we explore different embedding dimensions and provide a plot showing the relationship between epoch count and accuracy. The full details of the experiments are presented in the appendix.

5.2 Experimental Results

The experimental results, presented in Table 2, highlight the superior performance of our proposed method across various models and datasets. The most significant improvement is observed when employing our method with neural networks, where we achieved the highest accuracy across all three datasets—0.3052, 0.4793, and 0.2309 for LSHTC1, DMOZ, and ODP, respectively. This outperforms the standard cross entropy and squared loss methods, emphasizing the effectiveness of our approach. Note that the cross entropy loss achieves better performance as we found that it achieves higher accuracy with much larger batch sizes. This phenomenon is not observed on other datasets. When

utilizing elastic net or random forest models, our method demonstrated a significant reduction in training time while maintaining competitive accuracy levels. Comparing linear methods, the JOLLE elastic net implementations outperform PD-Sparse and PPD-Sparse in both accuracy and training speed. The random forest models offer a trade-off point between linear models and neural networks in terms of accuracy and training time. This comprehensive comparison underscores the robustness of our method, providing a balance between accuracy and computational efficiency across different models and datasets. The experimental results emphasize the potential of our proposed method in tackling extreme multiclass classification problems effectively and efficiently.

As demonstrated in Figures 1, 2, and 3, our methods introduce new trade-off points in extreme multiclass classification. On one hand, our methods can achieve speed improvements with a marginal compromise in accuracy. This is particularly beneficial for time-sensitive applications or when dealing with massive datasets where computational resources are limited. On the other hand, when the priority is maximized accuracy, our methods can still deliver, outperforming competing models while necessitating increased runtime. These flexible trade-offs underscore the adaptability of our techniques to a wide range of practical scenarios, providing valuable alternatives in the toolkit for tackling extreme multiclass classification problems.

We compare our framework with varying embedding dimensions against neural networks employing both the standard cross-entropy loss and squared loss on a GPU. The results, as depicted in Figures 4, 5, and 6, demonstrate the robust performance of our method in terms of accuracy and a notably accelerated convergence speed. For the LSHTC1 dataset, we allow the cross entropy baseline to train a few more epochs to fully converge. In particular, JOLLE achieves superior performance in contrast to the standard cross-entropy and squared loss approaches. As evidenced by the research of Zhai and Wang (2018), there exists a linear relationship between the dimension of the output space and the generalization error bound. Therefore, it can be inferred that the enhanced performance of our method may be attributed to the reduction in the generalization error, a direct consequence of dimensionality reduction.

Method		Dataset		
		LSHTC1	DMOZ	ODP
PD-Sparse (Single Node)	Accuracy	0.2210	0.3970	N/A
	Time	230s	829s	> 50 hrs
PPD-Sparse (Multiple Nodes)	Accuracy	0.2260	0.3930	0.1366
	Time	135s	656s	668s
WLSTS (Single Node)	Accuracy	0.1640	N/A	N/A
	Time	12660s	> 20 hrs	> 28 hrs
AnnexML (Single Node)	Accuracy	0.2934	0.3972	0.2164
	Time	424s	2072s	10435s
Parabel (Single Node)	Accuracy	0.2224	0.3856	0.1709
	Time	96s	600s	1943s
JOLLE (Elastic Net, Single Node, $n = 360$)	Accuracy	0.2342	0.4109	0.1511
	Time	55s	254s	2045s
JOLLE (Elastic Net, Distributed, $n = 360$)	Accuracy	0.2338	0.4057	0.1506
	Time	14s	68s	350s
JOLLE (Random Forest, Single Node, $n = 360$)	Accuracy	0.2582	0.3265	0.1660
	Time	482s	1799s	2293s
JOLLE (Random Forest, Distributed, $n = 360$)	Accuracy	0.2664	0.3585	0.1660
	Time	63s	226s	359s
JOLLE (Neural Networks, GPU, $n = 512$)	Accuracy	0.3052	0.4793	0.2309
	Time	2260s	5886s	14590s
Standard Cross Entropy (GPU)	Accuracy	0.2940	0.4688	0.1720
	Time	529s	5935s	17374s
Standard Squared Loss (GPU)	Accuracy	0.2804	0.3798	0.1858
	Time	2301s	5934s	17635s

Table 2: Comparison of accuracy and training time across different methods and datasets. Each method has two entries, one for accuracy and one for training time.

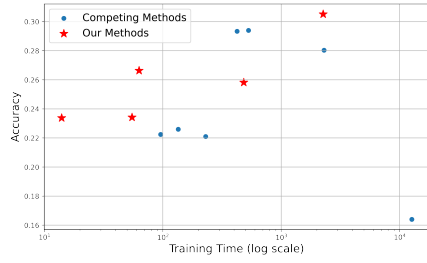


Figure 1: Plot of training time (log scale) vs accuracy for the LSHTC1 dataset.

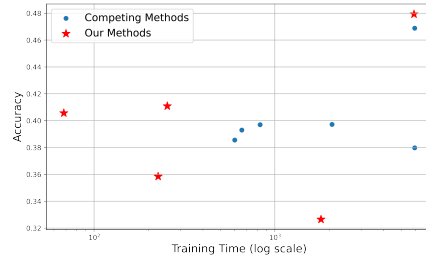


Figure 2: Plot of training time (log scale) vs accuracy for the Dmoz dataset.

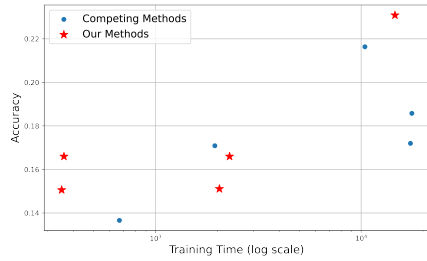


Figure 3: Plot of training time (log scale) vs accuracy for the ODP dataset.

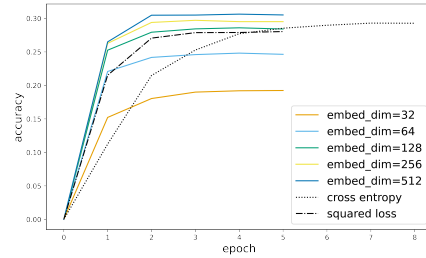


Figure 4: Plot of epoch vs accuracy for the LSHTC1 dataset.

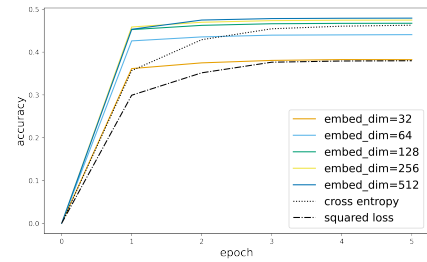


Figure 5: Plot of epoch vs accuracy for the Dmoz dataset.

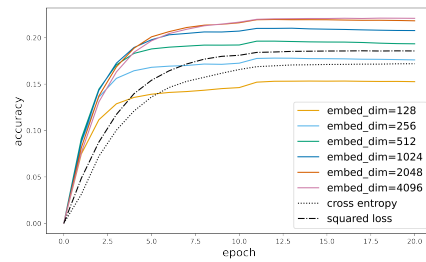


Figure 6: Plot of epoch vs accuracy for the ODP dataset.

6 Conclusion and Future Work

In conclusion, we have proposed a theory-grounded embedding approach for extreme multiclass classification. Our analysis offers a deeper understanding of the trade-offs between dimensionality reduction and the potential penalty in accuracy. We derived an excess risk bound that reveals a small penalty for dimensionality reduction and that this penalty vanishes under the multiclass Massart condition. Through extensive experiments, we demonstrated that our method outperforms state-of-the-art techniques in both accuracy and run time.

An interesting and immediate application is to extend the analysis to multilabel classification. Several avenues for future work include extending our framework to online learning scenarios, where adding an embedding dimension and scaling existing regressors can accommodate new classes as they emerge. Another potential extension involves learning with rejection, which would allow the model to reject samples with low confidence, thereby improving overall performance. Our embedding approach offers a promising direction for tackling extreme multiclass classification problems, contributing to a more robust understanding of the underlying trade-offs and providing a solid foundation for future research in this area.

Acknowledgment This work was supported in part by the National Science Foundation under award 2008074 and the Department of Defense, Defense Threat Reduction Agency under award HDTRA1-20-2-0002.

References

- Allwein, E. L., Schapire, R. E., and Singer, Y. (2001). Reducing Multiclass to Binary: A Unifying Approach for Margin Classifiers. *J. Mach. Learn. Res.*, 1:113–141.
- Babbar, R. and Schölkopf, B. (2017). DiSMEC: Distributed Sparse Machines for Extreme Multi-Label Classification. In *Proceedings of the Tenth ACM International Conference on Web Search and Data Mining, WSDM '17*, page 721–729, New York, NY, USA. Association for Computing Machinery.
- Babbar, R. and Schölkopf, B. (2019). Data scarcity, robustness and extreme multi-label classification. *Machine Learning*, 108.
- Bhatia, K., Jain, H., Kar, P., Varma, M., and Jain, P. (2015). Sparse Local Embeddings for Extreme Multi-label Classification. In Cortes, C., Lawrence, N., Lee, D., Sugiyama, M., and Garnett, R., editors, *Advances in Neural Information Processing Systems*, volume 28. Curran Associates, Inc.
- Chang, W.-C., Yu, H.-F., Zhong, K., Yang, Y., and Dhillon, I. S. (2019). A Modular Deep Learning Approach for Extreme Multi-label Text Classification. *ArXiv*, abs/1905.02331.
- Choromanska, A. E. and Langford, J. (2015). Logarithmic Time Online Multiclass prediction. In Cortes, C., Lawrence, N., Lee, D., Sugiyama, M., and Garnett, R., editors, *Advances in Neural Information Processing Systems*, volume 28. Curran Associates, Inc.
- Dahiya, K., Saini, D., Mittal, A., Dave, K., Jain, H., Agarwal, S., and Varma, M. (2021). Deep-XML: A deep extreme multi-Label learning framework applied to short text documents. In *ACM International Conference on Web Search and Data Mining*.
- Deng, H., Han, J., Zhao, Z., and Liu, H. (2018). Dual principal component pursuit: Improved analysis and efficient algorithms. In *Advances in Neural Information Processing Systems*, pages 1514–1524.
- Evron, I., Moroshko, E., and Crammer, K. (2018). Efficient Loss-Based Decoding on Graphs for Extreme Classification. In Bengio, S., Wallach, H., Larochelle, H., Grauman, K., Cesa-Bianchi, N., and Garnett, R., editors, *Advances in Neural Information Processing Systems*, volume 31. Curran Associates, Inc.
- Guo, C., Mousavi, A., Wu, X., Holtmann-Rice, D. N., Kale, S., Reddi, S., and Kumar, S. (2019). Breaking the Glass Ceiling for Embedding-Based Classifiers for Large Output Spaces. In Wallach, H., Larochelle, H., Beygelzimer, A., d'Alché-Buc, F., Fox, E., and Garnett, R., editors, *Advances in Neural Information Processing Systems*, volume 32. Curran Associates, Inc.
- Gupta, N., Chen, P., Yu, H.-F., Hsieh, C.-J., and Dhillon, I. (2022). ELIAS: End-to-End Learning to Index and Search in Large Output Spaces. In Koyejo, S., Mohamed, S., Agarwal, A., Belgrave, D., Cho, K., and Oh, A., editors, *Advances in Neural Information Processing Systems*, volume 35, pages 19798–19809. Curran Associates, Inc.
- Hsu, D., Kakade, S. M., Langford, J., and Zhang, T. (2009). Multi-Label Prediction via Compressed Sensing. In *Proceedings of the 22nd International Conference on Neural Information Processing Systems, NIPS'09*, page 772–780, Red Hook, NY, USA. Curran Associates Inc.
- Jain, H., Balasubramanian, V., Chunduri, B., and Varma, M. (2019). Slice: Scalable Linear Extreme Classifiers trained on 100 Million Labels for Related Searches. In *WSDM '19, February 11–15, 2019, Melbourne, VIC, Australia*. ACM. Best Paper Award at WSDM '19.
- Jernite, Y., Choromanska, A., and Sontag, D. (2017). Simultaneous Learning of Trees and Representations for Extreme Classification and Density Estimation. In Precup, D. and Teh, Y. W., editors, *Proceedings of the 34th International Conference on Machine Learning*, volume 70 of *Proceedings of Machine Learning Research*, pages 1665–1674. PMLR.

- Jiang, T., Wang, D., Sun, L., Yang, H., Zhao, Z., and Zhuang, F. (2021). LightXML: Transformer with Dynamic Negative Sampling for High-Performance Extreme Multi-label Text Classification. *Proceedings of the AAAI Conference on Artificial Intelligence*, 35(9):7987–7994.
- Johnson, W. B. and Lindenstrauss, J. (1984). Extensions of Lipschitz mappings into Hilbert space. *Contemporary mathematics*, 26:189–206.
- Khandagale, S., Xiao, H., and Babbar, R. (2020). Bonsai: Diverse and Shallow Trees for Extreme Multi-Label Classification. *Mach. Learn.*, 109(11):2099–2119.
- Le, Q. and Mikolov, T. (2014). Distributed representations of sentences and documents. In *International conference on machine learning*, pages 1188–1196. PMLR.
- Massart, P. and Nédélec, E. (2006). Risk Bounds for Statistical Learning. *The Annals of Statistics*, 34(5):2326–2366.
- Medini, T. K. R., Huang, Q., Wang, Y., Mohan, V., and Shrivastava, A. (2019). Extreme Classification in Log Memory using Count-Min Sketch: A Case Study of Amazon Search with 50M Products. In Wallach, H., Larochelle, H., Beygelzimer, A., d'Alché-Buc, F., Fox, E., and Garnett, R., editors, *Advances in Neural Information Processing Systems*, volume 32. Curran Associates, Inc.
- Prabhu, Y., Kag, A., Harsola, S., Agrawal, R., and Varma, M. (2018). Parabel: Partitioned Label Trees for Extreme Classification with Application to Dynamic Search Advertising. In *ACM International WWW Conference*, pages 993–1002. International World Wide Web Conferences Steering Committee, International World Wide Web Conferences Steering Committee.
- Prabhu, Y. and Varma, M. (2014). FastXML: A Fast, Accurate and Stable Tree-Classifier for Extreme Multi-Label Learning. In *Proceedings of the 20th ACM SIGKDD International Conference on Knowledge Discovery and Data Mining*, KDD '14, page 263–272, New York, NY, USA. Association for Computing Machinery.
- Ramaswamy, H. G., Tewari, A., and Agarwal, S. (2018). Consistent algorithms for multiclass classification with an abstain option. *Electronic Journal of Statistics*, 12(1):530 – 554.
- Tagami, Y. (2017). AnnexML: Approximate Nearest Neighbor Search for Extreme Multi-Label Classification. In *Proceedings of the 23rd ACM SIGKDD International Conference on Knowledge Discovery and Data Mining*, KDD '17, page 455–464, New York, NY, USA. Association for Computing Machinery.
- Wei, T., Tu, W.-W., and Li, Y.-F. (2019). Learning for Tail Label Data: A Label-Specific Feature Approach. In *Proceedings of the 28th International Joint Conference on Artificial Intelligence*, IJCAI'19, page 3842–3848. AAAI Press.
- Yen, I. E., Huang, X., Dai, W., Ravikumar, P., Dhillon, I., and Xing, E. (2017). PPDsparse: A Parallel Primal-Dual Sparse Method for Extreme Classification. In *Proceedings of the 23rd ACM SIGKDD International Conference on Knowledge Discovery and Data Mining*, KDD '17, page 545–553, New York, NY, USA. Association for Computing Machinery.
- Yen, I. E.-H., Huang, X., Ravikumar, P., Zhong, K., and Dhillon, I. (2016). PD-Sparse : A Primal and Dual Sparse Approach to Extreme Multiclass and Multilabel Classification. In Balcan, M. F. and Weinberger, K. Q., editors, *Proceedings of The 33rd International Conference on Machine Learning*, volume 48 of *Proceedings of Machine Learning Research*, pages 3069–3077, New York, New York, USA. PMLR.
- You, R., Zhang, Z., Wang, Z., Dai, S., Mamitsuka, H., and Zhu, S. (2019). *AttentionXML: Label Tree-Based Attention-Aware Deep Model for High-Performance Extreme Multi-Label Text Classification*. Curran Associates Inc., Red Hook, NY, USA.
- Yu, H.-F., Jain, P., Kar, P., and Dhillon, I. S. (2014). Large-scale multi-label learning with missing labels. In *Proceedings of the 31st International Conference on International Conference on Machine Learning - Volume 32*, ICML'14, page I–593–I–601. JMLR.org.
- Yu, H.-F., Zhong, K., Zhang, J., Chang, W.-C., and Dhillon, I. S. (2022). PECOS: Prediction for enormous and correlated output spaces. *Journal of Machine Learning Research*.

- Zhai, K. and Wang, H. (2018). Adaptive dropout with rademacher complexity regularization. In *International Conference on Learning Representations*.
- Zhang, J., Chang, W.-C., Yu, H.-F., and Dhillon, I. (2021). Fast Multi-Resolution Transformer Fine-tuning for Extreme Multi-label Text Classification. In Ranzato, M., Beygelzimer, A., Dauphin, Y., Liang, P., and Vaughan, J. W., editors, *Advances in Neural Information Processing Systems*, volume 34, pages 7267–7280. Curran Associates, Inc.
- Zhou, D.-X., Tang, J., and Yang, Y. (2014). Large scale multi-label learning with missing labels. In *International Conference on Machine Learning*, pages 593–601. PMLR.

A Experiment Details

In this section, we provide the details of our experiments.

A.1 Elastic Net

We aim to solve

$$\min_{W \in \mathbb{R}^{D \times n}} \|XW - Y\|_{fro}^2 + \lambda_1 \|W\|_{1,1} + \lambda_2 \|W\|_{fro}^2, \quad (5)$$

where $X \in \mathbb{R}^{N \times D}$ is the data matrix, the rows of $Y \in \mathbb{R}^{N \times n}$ are embedding vectors.

The problem (5) can be broken down into n independent real-output regression problems of the form

$$\min_{W_j \in \mathbb{R}^D} \|XW_j - Y_j\|_{fro}^2 + \lambda_1 \|W_j\|_1 + \lambda_2 \|W_j\|_2^2,$$

where W_j is the j -th column of W and Y_j is the j -th column of Y . Consequently, We can distribute the n real-output regression problems across multiple cores.

We develop a regression variant of the Fully-Corrective Block-Coordinate Frank-Wolfe (FC-BCFW) algorithm (Yen et al., 2016) and use it to solve the real-output regression problems. As the solver operates iteratively, we set it to run for a predefined number of iterations, denoted as N_{iter} . The chosen hyperparameters are outlined in table 3.

Dataset	λ_1	λ_2	N_{iter}
LSHTC1	0.1	1	20
DMOZ	0.01	0.01	20
ODP	0.01	0.1	40

Table 3: Hyperparameters for elastic net.

A.2 Random Forest

In this part of the implementation, we employ the standard random forest regression. Different from the elastic net, we distribute trees across multiple cores rather than distributing output dimensions. This distribution strategy suits random forests as a considerable portion of the training time is consumed by sorting data during the splitting process.

We set the maximum tree depth for all datasets to 100,000, effectively allowing the trees to have unbounded depth. We stop splitting when a node has fewer than 10 data points and we ensure every leaf node contains at least 5 data points. The number of features we consider for each split varies with the datasets: for DMOZ and LSHTC1, we look at 4000 features, while for ODP, considering its size, we restrict to 650 features in each split to ensure a reasonable runtime. The chosen hyperparameters are outlined in Table 4.

Dataset	Max Depth	Min Leaf Size	Min Split Size	# Features
LSHTC1	100,000	5	10	4000
DMOZ	100,000	5	10	4000
ODP	100,000	5	10	650

Table 4: Hyperparameters for the Random Forest implementation.

A.3 Neural Networks

In this section, we provide details on the architectures and hyperparameter choices for the neural networks used in our experiments. The architectures and hyperparameters are selected by trial-and-error on a heldout dataset.

A.3.1 LSHTC1

The proposed embedding strategy adopts a 2-layer neural network architecture, employing a hidden layer of 4096 neurons with ReLU activation. The output of the neural network is normalized to

have a Euclidean norm of 1 since the embedding vectors typically have a Euclidean norm close to 1. An Adamax optimizer with a learning rate of 0.001 is utilized together with a batch size of 128 for training. The model is trained for a total of 5 epochs. In order to effectively manage the learning rate, a scheduler is deployed, which scales down the learning rate by a factor of 0.1 at the second epoch.

Our cross-entropy baseline retains a similar network architecture to the embedding strategy, with an adjustment in the output layer to reflect the number of classes. Here, the learning rate is 0.01 and the batch size is increased to 2048 for training. The model undergoes training for a total of 10 epochs, with a scheduler set to decrease the learning rate after the fifth epoch.

Finally, the squared loss baseline follows the architecture of our cross-entropy baseline, with the learning rate and batch size mirroring the parameters of the embedding strategy. As with the embedding strategy, the output is normalized. The model is trained for a total of 5 epochs, and the learning rate is scheduled to decrease after the third epoch.

A.3.2 DMOZ

For the DMOZ dataset, our proposed label embedding strategy employed a 2-layer neural network with a hidden layer of 2500 neurons activated by the ReLU function. The output of the network is normalized to have a norm of 1. We trained the model using the Adamax optimizer with a learning rate of 0.001 and a batch size of 256. The model was trained for 5 epochs, and the learning rate was scheduled to decrease at the second and fourth epochs by a factor of 0.1.

For the cross-entropy loss baseline, we used the same network architecture with an adjustment in the output layer to match the number of classes. The learning rate was 0.01 and the batch size was 256. The model underwent training for a total of 5 epochs, with the learning rate decreasing after the third epoch as determined by the scheduler.

Lastly, the squared loss baseline utilized the same architecture, learning rate, and batch size as the proposed label embedding strategy. Similarly, the model’s output was normalized. The model was trained for 5 epochs, with the learning rate scheduled to decrease after the third epoch.

A.3.3 ODP

For the ODP dataset, the experiments utilized a neural network model composed of 4 layers. The size of the hidden layers progressively increased from 2^{10} to 2^{14} , then decreased to 2^{13} . Each of these layers employed the ReLU activation function and was followed by batch normalization to promote faster, more stable convergence. The final layer output size corresponded with the embedding dimension for the label embedding strategy and the number of classes for the cross-entropy and squared loss baselines.

In the label embedding framework, the output was normalized to yield a norm of 1. This model was trained using the Adamax optimizer, a learning rate of 0.001, and a batch size of 2048. The training spanned 20 epochs, with a learning rate decrease scheduled after the 10th epoch by a factor of 0.1.

For the cross-entropy loss baseline, the same network architecture was preserved, with an adjustment to the penultimate layer, reduced by half, and the final output layer resized to match the number of classes. This slight modification in the penultimate layer was necessary to accommodate the models within the 48GB GPU memory. Notably, the neural network output was normalized by dividing each output vector by its Euclidean norm before applying the softmax function, a non-standard operation that significantly enhanced performance. This model was trained using a learning rate of 0.01 over 20 epochs, following a similar learning rate schedule.

Finally, the squared loss baseline used the same architecture as the cross-entropy baseline and the same learning rate and batch size as the label embedding model. Here, the output was also normalized. The model underwent training for 20 epochs, with a learning rate decrease scheduled after the 10th epoch.

B Proof of Theorem 3

Recall that $\beta(p) = \min\{\arg \min_{i \in \mathcal{Y}} \|p - g_i\|_2\}$.

Lemma 7. $\forall p \in \mathbb{R}^n, \forall x \in \mathcal{X}, C_{1,x}(p) = \max_i \eta_i(x) - \eta_{\beta(p)}(x)$.

Proof. Recall that $L(p, y) = L_{01}(\beta(p), y) = \mathbb{1}_{\{\min\{\arg \min_{i \in \mathcal{Y}} \|p - g_i\|_2\} \neq y\}}$. The result follows from the observation that $C_{L,x}(p) = 1 - \eta_{\beta(p)}(x)$ and $C_{L,x}^* = 1 - \max_i \eta_i(x)$. \square

Lemma 8. $C_{2,x}$ is strictly convex and minimized at $p_x^* = G\eta(x) = \sum_{i=1}^C \eta_i(x)g_i$.

Proof.

$$\begin{aligned} C_{\ell,x}(p) &= \mathbb{E}_{y \sim P_{Y|X=x}} \ell(p, g(y)) \\ &= \frac{1}{2} \sum_{i=1}^C \eta_i(x) \|p - g(i)\|_2^2 \\ &= \frac{1}{2} \sum_{i=1}^C \eta_i(x) \langle p - g(i), p - g(i) \rangle \\ &= \frac{1}{2} \langle p, p \rangle - \left\langle \sum_{i=1}^C \eta_i(x) g(i), p \right\rangle + \frac{1}{2} \sum_{i=1}^C \eta_i(x) \|g(i)\|_2^2 \end{aligned}$$

So $DC_{2,x}(p) = p - \sum_{i=1}^C \eta_i(x)g(i)$ and $HC_{2,x}(p) = I$ where D stands for derivative and H stands for Hessian. \square

We'll use p_x^* to denote $G\eta(x)$ henceforward.

Lemma 9. Let $u : S \subset \mathbb{R}^n \rightarrow \mathbb{R}$ be a continuous strictly convex function where S is a convex set with non-empty interior. Let u be minimized at x^* with $u(x^*) = 0$. $\forall \delta_0 > 0, \exists \delta > 0$ such that $u(x) < \delta \implies \|x - x^*\|_2 < \delta_0$. A choice of such δ is $\inf_{x: \|x - x^*\|_2 = \delta_0} u(x)$.

Proof. We first confirm the fact that $\forall t \in (0, 1)$ and $q \in S - \{0\}$, $u(x^* + tq) < u(x^* + q)$.

$$\begin{aligned} u(x^* + tq) &= u((1-t)x^* + t(x^* + q)) \\ &< (1-t)u(x^*) + tu(x^* + q) \\ &= tu(x^* + q) \\ &< u(x^* + q). \end{aligned}$$

Let $\delta = \inf_{x: \|x - x^*\|_2 = \delta_0} u(x)$. Assume the opposite: $u(x) < \delta$ and $\|x - x^*\|_2 \geq \delta_0$. Then

$$u(x) = u(x^* + (x - x^*)) \geq u(x^* + \frac{\delta_0}{\|x - x^*\|} (x - x^*)) \geq \delta,$$

which results in a contradiction. Hence, $u(x) < \delta \implies \|x - x^*\|_2 < \delta_0$. \square

Lemma 10. Fix $x \in \mathcal{X}$, $\forall \delta_0 > 0 \forall p \in \mathbb{R}^n$, $C_{2,x}(p) < \frac{1}{2}\delta_0^2 \implies \|p - p_x^*\| < \delta_0$.

Proof. Applying Lemma 9 with $u = C_{2,x}$, $S = \mathbb{R}^n$, and $x^* = p_x^*$, we have $\forall p \in \mathbb{R}^n$, $C_{2,x}(p) < \inf_{s: \|s - p_x^*\|_2 = \delta_0} C_{2,x}(s) \implies \|p - p_x^*\|_2 < \delta_0$. Thus,

$$\begin{aligned} \inf_{s: \|s - p_x^*\|_2 = \delta_0} C_{2,x}(s) &= \inf_{s: \|s - p_x^*\|_2 = \delta_0} \left(\frac{1}{2} \langle s, s \rangle - \langle p_x^*, s \rangle \right) - \left(\frac{1}{2} \langle p_x^*, p_x^* \rangle - \langle p_x^*, p_x^* \rangle \right) \\ &= \inf_{s: \|s - p_x^*\|_2 = \delta_0} \frac{1}{2} \|s - p_x^*\|_2^2 \\ &= \frac{1}{2} \delta_0^2. \end{aligned}$$

\square

To facilitate our proofs, we define the Johnson-Lindenstrauss property as follows. Note that Johnson-Lindenstrauss property is a definition on fixed matrices and Johnson-Lindenstrauss matrices are matrices that satisfy the Johnson-Lindenstrauss property with high probability.

Definition 11. A matrix $G \in \mathbb{R}^{C \times n}$ satisfies the Johnson-Lindenstrauss property with parameters ϵ and m , if $\forall m$ -element subsets $V \subset \mathbb{R}^n$, $\forall v, v' \in V$, $|\langle Gv, Gv' \rangle - \langle v, v' \rangle| \leq \epsilon \|v\| \|v'\|$. We denote the set of all matrices satisfying the Johnson-Lindenstrauss property with parameters ϵ and m by $JLP(\epsilon, m)$.

Lemma 12. If $G \in JLP(\epsilon, m)$, then $\forall \eta \in \Delta^C$ and $\forall j \in [C]$,

$$\|\eta - e_j\|_2^2 - \epsilon \leq \|G(\eta - e_j)\|_2^2 \leq \|\eta - e_j\|_2^2 + \epsilon,$$

where $\{e_i : i \in [C]\}$ is the standard basis of \mathbb{R}^C .

Proof. Since $G \in JLP(\frac{\epsilon}{4}, \delta, C)$, $\|Ge_i\|_2^2 \in [1 - \frac{\epsilon}{4}, 1 + \frac{\epsilon}{4}]$ and for $i \neq j$, $\langle Ge_i, Ge_j \rangle \in [-\frac{\epsilon}{4}, \frac{\epsilon}{4}]$.

Write $\eta^{(j)} = \eta - e_j$.

$$\begin{aligned} \|G\eta - Ge_j\|_2^2 &= \|G\eta^{(j)}\|_2^2 \\ &= \left\| \sum_{i=1}^C \eta_i^{(j)} Ge_i \right\|_2^2 \\ &= \sum_{i=1}^C |\eta_i^{(j)}|^2 \|Ge_i\|_2^2 + \sum_{\substack{i, i'=1 \\ i \neq i'}}^C \eta_i^{(j)} \eta_{i'}^{(j)} \langle Ge_i, Ge_{i'} \rangle. \end{aligned}$$

Then

$$\begin{aligned} (1 - \frac{\epsilon}{4}) \sum_{i=1}^C |\eta_i^{(j)}|^2 - \frac{\epsilon}{4} \sum_{\substack{i, i'=1 \\ i \neq i'}}^C |\eta_i^{(j)}| |\eta_{i'}^{(j)}| &\leq \|G\eta - Ge_j\|_2^2 \\ &\leq (1 + \frac{\epsilon}{4}) \sum_{i=1}^C |\eta_i^{(j)}|^2 + \frac{\epsilon}{4} \sum_{\substack{i, i'=1 \\ i \neq i'}}^C |\eta_i^{(j)}| |\eta_{i'}^{(j)}|. \end{aligned}$$

Write

$$U = (1 - \frac{\epsilon}{4}) \sum_{i=1}^C |\eta_i^{(j)}|^2 - \frac{\epsilon}{4} \sum_{\substack{i, i'=1 \\ i \neq i'}}^C |\eta_i^{(j)}| |\eta_{i'}^{(j)}|$$

and

$$L = (1 + \frac{\epsilon}{4}) \sum_{i=1}^C |\eta_i^{(j)}|^2 + \frac{\epsilon}{4} \sum_{\substack{i, i'=1 \\ i \neq i'}}^C |\eta_i^{(j)}| |\eta_{i'}^{(j)}|.$$

These can be simplified as $L = \|\eta^{(j)}\|_2^2 - \frac{\epsilon}{4} \|\eta^{(j)}\|_1^2$ and $U = \|\eta^{(j)}\|_2^2 + \frac{\epsilon}{4} \|\eta^{(j)}\|_1^2$. Note that $\|\eta^{(j)}\|_2^2 = \|\eta\|_2^2 - 2\eta_j + 1$.

As $\|\eta^{(j)}\|_1 = 2 - 2\eta_j < 2$, $L > \|\eta^{(j)}\|_2^2 - \epsilon$ and $U < \|\eta^{(j)}\|_2^2 + \epsilon$. \square

Lemma 13. If $G \in JLP(\epsilon, m)$, then $\forall x \in \mathcal{X}$, $\forall j, k \in [C]$, $\forall p \in \mathbb{R}^n$,

$$\frac{\eta_k(x) - \eta_j(x) - \epsilon}{2\sqrt{2} + \epsilon} > \|p_x^* - p\| \implies \|p - g_j\|_2 > \|p - g_k\|_2.$$

Proof. Write $p = p_x^* + \delta_0 v$ where $v = \frac{p - p_x^*}{\|p - p_x^*\|}$ and $\delta_0 = \|p - p_x^*\|$. Recall that $\{e_i\}$ is the standard basis of \mathbb{R}^C and that $p_x^* = G\eta(x)$.

$$\begin{aligned} & \frac{(\eta_k(x) - \eta_j(x)) - \epsilon}{2\sqrt{2 + \epsilon}} > \delta_0 \\ \implies & 2(\eta_k(x) - \eta_j(x)) - 2\epsilon > 4\delta_0\sqrt{2 + \epsilon} \\ \implies & \left(\|\eta(x)\|^2 - 2\eta_j(x) + 1 - \epsilon \right) - \left(\|\eta(x)\|^2 - 2\eta_k(x) + 1 + \epsilon \right) > \\ & 2\delta_0\sqrt{\|\eta(x)\|^2 - 2\eta_j(x) + 1 + \epsilon} + 2\delta_0\sqrt{\|\eta(x)\|^2 - 2\eta_k(x) + 1 + \epsilon} \end{aligned} \quad (6)$$

$$\begin{aligned} \implies & \left(\|\eta(x) - e_j\|_2^2 - \epsilon \right) - \left(\|\eta(x) - e_k\|_2^2 + \epsilon \right) > \\ & 2\delta_0 \left(\sqrt{\|\eta(x) - e_k\|_2^2 + \epsilon} + \sqrt{\|\eta(x) - e_j\|_2^2 + \epsilon} \right) \\ \implies & \left(\|\eta(x) - e_j\|_2^2 - \epsilon \right) - 2\delta_0\sqrt{\|\eta(x) - e_j\|_2^2 + \epsilon} > \\ & \left(\|\eta(x) - e_k\|_2^2 + \epsilon \right) + 2\delta_0\sqrt{\|\eta(x) - e_k\|_2^2 + \epsilon} \\ \implies & \|G(\eta(x) - e_j)\|_2^2 - 2\delta_0\|G(\eta(x) - e_j)\|_2 + \delta_0^2 > \\ & \|G(\eta(x) - e_k)\|_2^2 + 2\delta_0\|G(\eta(x) - e_k)\|_2 + \delta_0^2 \end{aligned} \quad (7)$$

$$\begin{aligned} \implies & (\|G(\eta(x) - e_j)\|_2 - \delta_0\|v\|_2)^2 > (\|G(\eta(x) - e_k)\|_2 + \delta_0\|v\|_2)^2 \\ \implies & \|p_x^* + \delta_0 v - g_j\|_2^2 > \|p_x^* + \delta_0 v - g_k\|_2^2 \\ \implies & \|p - g_j\|_2^2 > \|p - g_k\|_2^2 \end{aligned} \quad (8)$$

Inequality (6) follows the observation that $\|\eta(x)\|^2 = \sum_i \eta_i^2(x) \leq \sum_i \eta_i(x) = 1$ and $\eta_i(x) \geq 0$. Inequality (7) is obtained by applying Lemma 12. Inequality (8) follows the triangle inequality. \square

Lemma 14. Let $G \in JLP(\frac{\epsilon}{4}, \delta, C)$. $\forall x \in \mathcal{X}, \forall r > \epsilon$, and $\forall p \in \mathbb{R}^n, C_{2,x}(p) < \frac{(r-\epsilon)^2}{16+8\epsilon} \implies C_{1,x}(p) < r$.

Proof. By Lemma 10, $C_{2,x}(p) < \frac{(r-\epsilon)^2}{16+8\epsilon} \implies \|p - p_x^*\| < \frac{r-\epsilon}{2\sqrt{2+\epsilon}}$. Fix $x \in \mathcal{X}$. Recall that $\beta(p) = \min\{\arg \min_{i \in \mathcal{Y}} \|p - g_i\|_2\}$.

We claim

$$\|p - p_x^*\| < \frac{r-\epsilon}{2\sqrt{2+\epsilon}} \implies \max_i \eta_i(x) - \eta_{\beta(p)}(x) < r.$$

Assume $\|p - p_x^*\| < \frac{r-\epsilon}{2\sqrt{2+\epsilon}}$ and $\max_i \eta_i(x) - \eta_{\beta(p)}(x) \geq r$. By Lemma 13 $\|p - g_{\beta(p)}\| > \|p - g_{\min\{\arg \max_i \eta_i(x)\}}\|$, contradicting the definition of $\beta(p)$.

Hence, $C_{1,x}(p) = \max_i \eta_i(x) - \eta_{\beta(p)}(x) < r$. \square

Now we're ready to prove Theorem 3.

Proof of Theorem 3.

$$\begin{aligned} \mathcal{R}_{L,P}(f) - \mathcal{R}_{L,P}^* &= \int_{\mathcal{X}} C_{1,x}(f(x)) \\ &= \int_{x:d(x)<r} C_{1,x}(f(x)) + \int_{x:d(x)\geq r} C_{1,x}(f(x)). \end{aligned}$$

We bound each integral individually.

By Lemma 14, $\forall x \in \mathcal{X}, \forall r > \epsilon$, and $\forall p \in \mathbb{R}^n$,

$$C_{1,x}(p) \geq r \implies C_{2,x}(p) \geq \frac{(r - \epsilon)^2}{16 + 8\epsilon}. \quad (9)$$

Hence,

$$\begin{aligned} C_{1,x}(p) > \epsilon &\implies C_{2,x}(p) \geq \frac{(C_{1,x}(p) - \epsilon)^2}{16 + 8\epsilon} \\ &\implies C_{1,x}(p) \leq \epsilon + \sqrt{(8\epsilon + 16)C_{2,x}(p)}. \end{aligned}$$

Note the last inequality actually holds for all $p \in \mathbb{R}^n$, that is, it holds even when $C_{1,x}(p) \leq \epsilon$. Then,

$$\begin{aligned} \int_{x:d(x)<r} C_{1,x}(f(x)) &\leq \int_{x:d(x)<r} \epsilon + \sqrt{(8\epsilon + 16)C_{2,x}(f(x))} \\ &= \int_{x:d(x)<r} \epsilon + \int_{x:d(x)<r} \sqrt{(8\epsilon + 16)C_{2,x}(f(x))} \\ &= \epsilon P_{\mathcal{X}}(d(X) < r) + \sqrt{(8\epsilon + 16)} \int_{x:d(x)<r} \sqrt{C_{2,x}(f(x))} \\ &= \epsilon P_{\mathcal{X}}(d(X) < r) + \sqrt{(8\epsilon + 16)} \left\| \mathbb{1}_{d(x)<r} \sqrt{C_{2,x}(f(x))} \right\|_{P_{\mathcal{X},1}} \\ &\leq \epsilon P_{\mathcal{X}}(d(X) < r) + \sqrt{(8\epsilon + 16)} \left\| \mathbb{1}_{d(x)<r} \right\|_{P_{\mathcal{X},2}} \left\| \sqrt{C_{2,x}(f(x))} \right\|_{P_{\mathcal{X},2}} \quad (10) \\ &= \epsilon P_{\mathcal{X}}(d(X) < r) + \sqrt{(8\epsilon + 16)} \sqrt{P_{\mathcal{X}}(d(X) < r)} \sqrt{\int_{x \in \mathcal{X}} C_{2,x}(f(x))} \\ &= \epsilon P_{\mathcal{X}}(d(X) < r) + \sqrt{(8\epsilon + 16)P_{\mathcal{X}}(d(X) < r)} (\mathcal{R}_{\ell,P}(f) - \mathcal{R}_{\ell,P}^*). \end{aligned}$$

In inequality (10), we apply Holder's inequality.

When $C_{1,x}(p) > 0$, $C_{1,x}(p) = \max_i \eta_i(x) - \eta_{\beta(p)}(x) \geq \max_i \eta_i(x) - \max_{i \notin \arg \max_j \eta_j(x)} \eta_i(x) = d(x)$. By (9), if $d(x) \geq r$ and $C_{1,x}(p) > 0$, then $C_{2,x}(p) \geq \frac{(r - \epsilon)^2}{16 + 8\epsilon}$. As $C_{1,x}(p) \in [0, 1]$, $d(x) \geq r$ and $C_{1,x}(p) > 0 \implies C_{2,x}(p) \geq \frac{(r - \epsilon)^2}{16 + 8\epsilon} C_{1,x}(p)$. It is trivial that $C_{2,x}(p) \geq \frac{(r - \epsilon)^2}{16 + 8\epsilon} C_{1,x}(p)$ also holds when $C_{1,x}(p) = 0$. Thus, $\forall x \in \mathcal{X}$ and $\forall p \in \mathbb{R}^n$, $d(x) \geq r \implies C_{2,x}(p) \geq \frac{(r - \epsilon)^2}{16 + 8\epsilon} C_{1,x}(p) \implies C_{1,x}(p) \leq \frac{16 + 8\epsilon}{(r - \epsilon)^2} C_{2,x}(p)$. Therefore,

$$\begin{aligned} \int_{x:d(x) \geq r} C_{1,x}(f(x)) &\leq \int_{x:d(x) \geq r} \frac{16 + 8\epsilon}{(r - \epsilon)^2} C_{2,x}(f(x)) \\ &\leq \frac{16 + 8\epsilon}{(r - \epsilon)^2} \int_{\mathcal{X}} C_{2,x}(f) \\ &= \frac{16 + 8\epsilon}{(r - \epsilon)^2} (\mathcal{R}_{\ell,P}(f) - \mathcal{R}_{\ell,P}^*) \end{aligned}$$

□